Journal of Colloid and Interface Science 699 (2025) 138149

Contents lists available at ScienceDirect

Journal of Colloid And Interface Science

journal homepage: www.elsevier.com/locate/jcis

Structural and mechanical scaling law behaviour in folded protein hydrogel networks

Ahmad Boroumand [a], Matt D.G. Hughes [a], Sophie Cussons [b,c], Najet Mahmoudi [d], David A. Head [e], Sally Peyman [f], Arwen I.I. Tyler [g], Lorna Dougan [a,b,*]

[a] School of Physics and Astronomy, Faculty of Engineering and Physical Sciences, University of Leeds, UK
[b] Astbury Centre for Structural Molecular Biology, University of Leeds, UK
[c] School of Molecular and Cellular Biology, Faculty of Biological Sciences, University of Leeds, UK
[d] ISIS Neutron and Muon Spallation Source, STFC Rutherford Appleton Laboratory, Oxfordshire, UK
[e] School of Computer Science, Faculty of Engineering and Physical Science, University of Leeds, UK
[f] School of Engineering and Physical Sciences, Institute of Biological Chemistry, Heriot Watt University, UK
[g] School of Food Science and Nutrition, Faculty of Environment, University of Leeds, UK

GRAPHICAL ABSTRACT

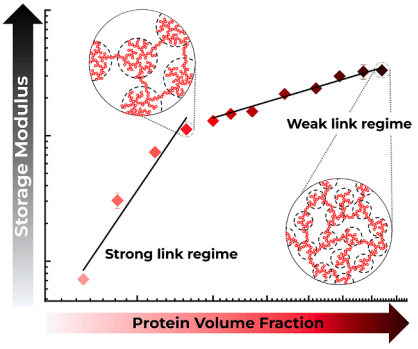

ARTICLE INFO

Keywords:
Colloidal networks
Polymer networks
Protein hydrogels
Rheology
Scaling laws
Small angle scattering
Scattering
Mechanics
Biomechanics
Hierarchical mechanics
Structure

ABSTRACT

Folded protein hydrogels are generating significant interest for their potential as functional biomaterials with tuneable properties. A detailed understanding of the relationship between their mechanics and structure would reveal their hierarchical design principles and provide rich opportunities for the design of biomaterials for specific medical and healthcare applications. Inspired by theories from soft matter physics, we have investigated the scaling behaviour of the protein volume fraction (ϕ) and its relationship to the underlying structure and mechanics of the protein network through a combination of rheology and small-angle neutron scattering (SANS). Using the globular protein bovine serum albumin (BSA) as a model system and photoactivated chemical cross-linking to retain the colloid-like folded protein structure, we have identified a two-regime behaviour in the storage moduli as a function of ϕ, reminiscent of the strong- and weak- link regimes in a colloidal flocculated model. SANS reveals a heterogeneous protein network structure with fractal-like clusters connected by inter-cluster regions. Network parameters such as the number of proteins in an average cluster and correlation length

* Corresponding author at: School of Physics and Astronomy, Faculty of Engineering and Physical Sciences, University of Leeds, UK.
E-mail address: L.Dougan@leeds.ac.uk (L. Dougan).

https://doi.org/10.1016/j.jcis.2025.138149
Received 4 February 2025; Received in revised form 15 May 2025; Accepted 8 June 2025
Available online 9 June 2025

scale with ϕ, in line with predictions from the de Gennes blob model. Such distinction between the mechanical and structural scaling relationships provides evidence of a cross-length scale behaviour where intercluster links are important in defining the macroscopic shear response of the system. Insights gained from our integrated structural and mechanical approach will support the future development of novel biomaterials which exploit the folded and functional properties of the protein building block and its responsiveness to mechanical and biochemical cues.

1. Introduction

Folded protein hydrogels are an emerging class of biomaterials with attractive viscoelastic properties and inherent biological functionality [1–4]. Previous studies have demonstrated that folded protein hydrogels can mimic the mechanical properties of cartilage and muscle [5,6], resembling dynamic and tunable elastic properties [7], and can be coupled with polymers to achieve enhanced mechanical function [8], thus lending themselves as attractive materials in bioengineering and healthcare applications. The hierarchical structure of folded protein hydrogels offers opportunities to build-by-design different macroscale systems with customised architectures for a specific need. In a recent example, a functional enzyme has been exploited as a hydrogel building block, allowing for the creation of a nanomachine network which is responsive to specific biochemical cues [2]. The geometry has been exploited to evolve and program biological materials [9–11] and recent work has shown that the morphology (shape) of the hydrogel building block is essential for efficient self-assembly [12]. Indeed, this has been explored in engineered protein networks comprised of repeating chains of protein building blocks of defined number and increasing aspect ratio, revealing their impact on protein network formation, architecture and mechanics [10]. In addition to geometry, photochemically crosslinked folded protein hydrogel systems offer a large design space for tuning biomaterial production, including protein volume fraction, crosslinking reaction rate, and choice of natural or synthetic protein building block. At the nanoscale protein level, the mechanical response of the protein can be manipulated to favour protein unfolding through the addition of chemical reducing reagents to break specific strong intramolecular covalent bonds within the protein and/or the addition of protein denaturants [5,8,13]. Protein unfolding can be manipulated to create an entangled protein network and bulk gel mechanics which are three times stronger than the folded protein network equivalent [14]. The mechanical properties of the protein network can also be manipulated through an increase in the stability of proteins [13,15]. The crosslinking reaction rate which triggers the formation of the protein hydrogel network can be tuned, for example, through the magnitude of the photoactivated light intensity, to achieve diffusion- and reaction-limited protein network assemblies [3,16]. The structure and mechanics of the folded protein hydrogels can be further tuned through control of the number of crosslinking sites, *i.e.*, valency on the protein building block or the number of protein domains in the polyprotein chain [17–19]. If we consider the structural architecture of folded protein hydrogels, studies using small-angle X-ray and neutron scattering have proposed a mesoscale network structure made up of heterogeneous regions of more densely packed fractal-like clusters interconnected by more sparsely populated chains of proteins [14,20], as illustrated in Fig. 1(A). More recently, cryo-scanning electron microscopy (cryoSEM) on folded protein hydrogels has revealed a heterogeneous network with nanoscale porosity surrounded by high secondary emission regions interconnected by narrower, lower emission regions [4]. Such networks are created through photo-initiated crosslinking between folded globular proteins, through the formation of irreversible, covalent dityrosine bonds on surface-accessible sites of the protein [3,14–16,20,21]. The application of a fractal structure factor model to scattering data [22] provides access to parameters such as fractal dimension (D) and correlation length, ξ. D is a measure of the geometric complexity of a self-similar object, and ξ is the maximum length scale above which clusters no longer appear fractal. By removing intramolecular protein nanostaples (covalent disulphide bonds) the protein becomes more force labile (more responsive to an applied force), resulting in protein unfolding and the formation of a different protein network topology. This includes more densely packed clusters (higher D) interconnected by a larger proportion of unfolded proteins [14], as confirmed by SANS and cryoSEM [4]. The network structure can be further manipulated by embedding microbubbles inside the crosslinked protein hydrogel, resulting in a network structure with reduced connections between fractal-like clusters [21]. Additionally, by tuning the protein building block aspect ratio the hydrogel network forms sparser clusters [10]. Indeed, as experimental

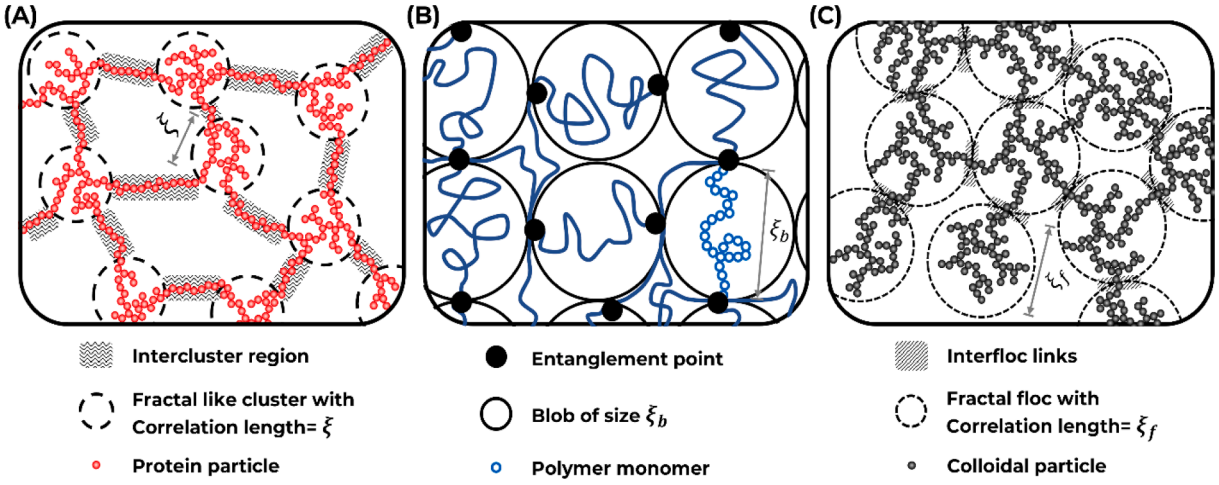

Fig. 1. Schematic to illustrate the analogy between folded protein hydrogels' structure and scaling laws in the literature. (**A**) The proposed structure of folded protein hydrogels. Globular BSA hydrogel forms denser areas that are fractal-like clusters linked via chains of particles. (**B**) Blob scaling theory initially proposed by de Gennes where polymer chains become entangled. The chain part between two entanglement points could be perceived as blob spheres and continue this process to fill up the whole network of blobs. (**C**) Aggregate of colloidal particles form fractal flocs that are interconnected via interfloc links.

tools continue to develop, the diversity of protein network properties increases [23].

While protein engineering [23–25], chemical crosslinking and composite systems [1,5,6,10] have successfully been employed to create a diversity of folded hydrogel networks with distinct viscoelastic properties, a simple method for tuning hydrogel mechanics is by changing the building block volume fraction, ϕ (the ratio of the volume of protein to the total volume of the solution, Supplementary Eq. (1)). This approach has been well utilised for a range of polymer and colloidal network systems and important theories have been developed to explain the observed scaling law dependencies. In soft matter physics, macromolecular conformations in equilibrium can be described by universal scaling laws [26,27] and are key for understanding structure, dynamics [28] and function of soft and biological matter [29,30]. Scaling laws are important in providing predictions of the behaviour of biopolymers under certain conditions and can provide valuable insights [31,32]. It is interesting to consider how the heterogenous network structures of folded protein hydrogels are related to colloidal and polymer assemblies. Indeed, adopting colloidal network theories for understanding protein assemblies has gained significant interest [33], for example in the application of the floc model to denatured (heat-induced or pH-induced crosslinking) protein hydrogels [34–36]. However, the applicability of colloidal network theories to chemically crosslinked folded protein hydrogels remains relatively unexplored.

The heterogeneous structural model of folded protein hydrogels is analogous to a number of theoretical models describing polymeric and colloidal flocculated systems (Fig. 1(B) and (C)) which relate the ϕ of the network building block to structural and mechanical properties of the network. One such model is the de Gennes' blob model [31] where, in the semidilute regime, chains of polymers overlap and form entanglement points (black filled circles in Fig. 1(B)). One can superimpose spheres on the distance between two adjacent entanglement points on the same chain called 'blobs' and continue to build up the whole system's structure, shown as circles surrounding the part of the chains of polymers in Fig. 1(B). The size of the blob, ξ_b is defined as the distance over which the density of monomers is higher than average. The region of the chain within a blob can take a convoluted fractal form with $D > 1$ even for a smooth curve. In the context of the blob model, the interconnected clusters of folded proteins in protein hydrogel networks (hatched area in Fig. 1(A)) could be interpreted as connected blobs which are more complex than a chain line [31,32]. Another model to consider is that of aggregated colloidal gels. Here, instead of entangled chains, particles aggregate into fractal flocs of size ξ_f (*i.e.*, ramified clusters of building block particles, depicted as dotted circles in Fig. 1(C)) that are interconnected into a network that spans space (hatched area in Fig. 1(C)) [37]. There is a similarity between the floc model and the mesoscale structure of folded protein hydrogels. The interconnected clusters of folded protein (Fig. 1(A)) could be equated to connected flocs (Fig. 1(C)) and the intercluster region to the interfloc links. Models described above relate structural and mechanical properties of the system's ϕ in a power law fashion known as scaling laws.

Polymer gels [38–42], colloidal gels [43–46], aggregated protein gels [34–36,47–51], capillary suspensions [37], and micellar systems [52,53] have demonstrated that a characteristic elastic constant K scales with the ϕ as:

$$K \sim \phi^{\mu} \tag{1}$$

with an exponent μ which is system-dependent; and is known to vary depending on the model used to describe the structure of the system. For example, for a network composed of elastic beams, the exponent is expected to be $\mu = 2$ [54], and the blob model predicts it to be $\mu = 2.25$ [31], while for worm-like chain polymers this is reported to be either $\mu = \frac{5}{2}$ or $\mu = \frac{11}{5}$ depending on whether it is a dense network or highly entangled, respectively [55]. For fractal colloids, this exponent is known to be a function of D [36,45,50].

Shih *et al.* developed a scaling theory for flocculated colloids in which the intrafloc and interfloc connective regions both had stiffnesses that scaled in different ways with ϕ [43]. Since disordered materials primarily deform in regions where the stiffness is low, they identified two regimes of mechanical response. A strong link (*i.e.*, weak floc) regime at low ϕ, where the material response is controlled by deformation in the large, sparse flocs; and a weak link (strong floc) regime at high ϕ where the response is instead controlled by the linkages between flocs. To distinguish between the different regimes, a parameter termed as the limit of linearity (γ_0) was introduced [43,56], defined as the first shear strain above which the system behaves non-linearly due to the breakage of bonds as the strain increases such that:

$$\gamma_0 \sim \phi^{\lambda} \tag{2}$$

This equation defines a new scaling exponent λ for γ_0 which is dependent on the weak- and strong- link regime. In the strong link regime (low ϕ), the mechanical response of the system is dominated by large flocs and showing a steeper power law:

$$\mu_{SL} = \frac{3+x}{3-D} \tag{3}$$

$$\lambda_{SL} = -\frac{1+x}{3-D} \tag{4}$$

where x, μ_{SL}, λ_{SL} are the fractal dimension of the load-carrying backbone of the flocs (Fig. 1(C)), the scaling law exponent of elastic modulus, and the power law exponent of the limit of linearity, respectively. Increasing the number of particles, *i.e.*, larger ϕ, causes a more gradual increase in the mechanics of the gels composed of weaker interfloc links, namely the weak link regime:

$$\mu_{WL} = \frac{1}{3-D} \tag{5}$$

$$\lambda_{WL} = \frac{1}{3-D} \tag{6}$$

In the equations above, μ_{WL} and λ_{WL} are the weak link exponents of the scaling law defined in Eqs. (1) and (2), respectively. Thus, in a ϕ dependent study, the slope of a logarithmic plot of the limit of linearity versus ϕ can reveal the appropriate weak and or strong link regime and guide the choice of using either Eq. (3) or Eq. (5) to obtain D. Hydrogels formed by aggregation of denatured proteins are reported to successfully follow the floc and interfloc link scaling model (Fig. 1(C)) [34,35,47–49,57,58]. However, the applicability of such models to covalently bound folded protein hydrogels is unknown.

Given the rich information now available on photochemically crosslinked folded protein hydrogels and the observed mesoscale structure [10,14,15,20,21] it is timely to consider their scaling behaviour. Such insight will improve our understanding of this emerging class of biomaterials [5,59–61] and help towards the development of theories to predict their properties. Here, we present a ϕ-dependent study of photochemically crosslinked BSA protein hydrogels using rheology and small angle scattering to obtain mechanical and structural information on the hydrogel networks. The scaling laws are identified in both the mechanics and structure of the system and considered in relation to current scaling theories.

2. Materials and methods

2.1. Materials

Ruthenium-tris(2,2′-bipyridyl) dichloride ($Ru(BPY)_3$), sodium peroxodisulfate (sodium persulphate), BSA (Heat shock fraction, protease-free, essentially globulin free, ≥98%), sodium phosphate monobasic, and sodium phosphate dibasic were purchased from Sigma Aldrich (Gillingham, UK). 10 mm path length match-paired Hellma quartz

cuvettes (104-10-K-40) were obtained from Scientific Laboratory Supplies (Nottingham, UK).

2.2. Hydrogel preparation

BSA was resuspended in sodium phosphate buffer (pH = 7.4) to make 200 mg/ml stocks. The BSA resuspension's concentration was measured after a 300x dilution in a cuvette-based UV/Vis/NIR spectrophotometer (Agilent Technologies Cary 5000 spectrophotometer) at 279 nm. To make the maximum volume fraction that is $\phi = 7.4\%$ (100 mg/ml), the crosslinker reagents contained 0.2 mM $Ru(BPY)_3$ and 100 mM sodium persulphate. The gel was made by 1:1 mixing of reagents and BSA stock solution. In order to make other ϕ samples, 200 mg/ml BSA stock solutions were diluted to the double value of the desired concentration, and mixed 1:1 with the reagents. For these samples, the sodium persulphate concentration in the reagent solution was changed to keep the molar ratio of sodium persulphate to BSA equal to that of the $\phi = 7.4\%$ sample (Supplementary Table 1). This approach keeps the molar ratio between protein tyrosine residues (crosslinking sites) and sodium persulphate constant for all samples and ensures the prevention of sodium persulphate overabundance (which can denature proteins) in low ϕ and incomplete crosslinking in higher ϕ.

Photoactivated chemically crosslinked hydrogels were formed using a protocol in which a lamp with an intensity and wavelength of 35.1 W/cm^2 of 452 nm was illuminated on the sample for 5 min to trigger network formation. For each experiment, the BSA stock solutions were made fresh.

2.3. Rheometry

Rheological measurements were conducted using an Anton Paar MCR 302 stress-controlled rheometer (Anton Paar GmbH, Austria). The lower plate was replaced by a custom-built *in situ* blue light LED lamp [16] and an upper 8 mm parallel plate geometry was used to ensure light reaches the samples with uniform intensity. First, the pre-gel solution (containing resuspended BSA and reagents) was added to the lower plate and then the gap size was set to 0.7 mm. To avoid evaporation of samples, silicon oil (5 cst) was added around the gel. At the beginning of the test, the lamp was kept off for 1 min and after that, it was turned on for 5 min. The measurements of shear and loss modulus as a function of time were done using a 0.5% shear rate and frequency of 1 Hz. Frequency dependency studies were done in the range of 0.1 to 1.33 Hz. All experiments were repeated in triplicates using fresh samples.

2.4. Small angle neutron scattering

SANS measurements were performed at the ISIS Neutron and Muon Source facility, on the Sans2d instrument with a collimation length of 12 m and a sample-to-detector distance of 5 and 12 m for the front and rear detector, respectively, achieving a scattering vector, q-range of 0.0015–0.5 $Å^{-1}$, with a q-resolution varying from ca. 2% at the highest q-values to ca. 19% with decreasing q-values, calculated using the Mildner Carpenter equation [62]. Samples were loaded into 2 mm quartz cuvettes and crosslinked using a 452 nm lamp. The remaining volume of the cuvettes was filled with buffer to prevent evaporation. The temperature of the sample holder was regulated to be at 20 ℃, using circulating water baths. Supplementary Fig. 1 shows the gels in cuvettes. All the samples were prepared in a 100% D_2O buffer. 2D raw images were radially averaged and corrected from the scattering of the empty cell and the scaled D_2O buffer. Detector efficiency corrections and absolute scaling of the data using a polymer standard were done using MANTID [63].

2.5. SANS data analysis

Shape-independent analysis was conducted using Guinier-Porod analysis in SasView 5.0.6 (http://www.sasview.org/). To obtain Porod exponents the whole range of data was used for fitting while only the q-range 0.0128 to 0.1074 $Å^{-1}$, (for objects bigger than single protein molecule) was analysed. Fitting for the chosen range is shown in Supplementary Fig. 2. For the radius of gyration (R_g) a q-range of 0.0015, 0.05 $Å^{-1}$ was defined by the upper limit of the Guinier approximation, $qR_g < 1-1.5$ (Supplementary Fig. 3) [64]. Guinier Porod analysis of $\phi =$ 2.2% (30 mg/ml solution of BSA) is shown in Supplementary Fig. 4 using the whole range for this fitting.

A fractal model was used to fit the whole q-range of the SANS data [14]. Briefly, this model uses an ellipsoid form factor ($F(q)$) to model BSA proteins and a structure factor ($S(q)$) describing fractal clustering of particles as:

$$F(q) = \left(\frac{3(sin(qr_e) - qrcos(qr_e))}{qr_e{}^3}\right)^2 \tag{7}$$

$$S(q) = \frac{D\Gamma(D-1)}{\left[1+\frac{1}{[q\xi]^2}\right]^{D-0.5}} \cdot \frac{\sin[(D-1)tan^{-1}(q\xi)]}{(qR_0)^D} \tag{8}$$

where r_e, R_0, and Γ are a radius term related to the polar radius and equatorial radius of the ellipsoid, the minimum cut-off length scale defined by the ellipsoid form factor, and the gamma function, respectively. Then, the scattering curve can be fitted by:

$$I(q) = \phi V_{block}\Delta\rho^2 F(q)[(1-P_c) + P_c S(q)] + background \tag{9}$$

where ϕ, V_{block}, $\Delta\rho$, and P_c are volume fraction of BSA protein, volume of the BSA as building block, contrast difference between protein and buffer, and proportion of proteins inside clusters, respectively. All fittings are provided in Supplementary Fig. 5. Example fitting parameters with their definitions are included in Supplementary Table 2.

A radial distribution function initially proposed by Sow-Hsin Chen and Teixeira [22] to describe the fractal structure factor was used to extract further network parameters:

$$g(r) = \frac{\rho_k D}{4\pi\phi r_0^D} r^{D-3} e^{-\frac{r}{\xi}} \tag{10}$$

where r_0 is the minimum cut-off distance of the fractal cluster and ρ_k is the maximum packing density of the system. This equation is used [14,21] to express the number of building block particles in a sphere of radius, r, from the centre of a cluster:

$$N(r) = \rho_k D\left(\frac{\xi}{r_0}\right)^D \gamma\left(D, \frac{r}{\xi}\right) \tag{11}$$

where, γ denotes the lower incomplete gamma function.

3. Results

3.1. Selection of a folded protein hydrogel model system

In this study, we chose BSA as the model building block due to its mechanical robustness with 17 covalent disulphide bonds. Folded BSA hydrogels were made by photoactivated crosslinking of BSA proteins using a method initially introduced by Fancy *et al.* [65] and depicted in Fig. 2. Briefly, the chemical reagents are added to the protein solution including a donor ($Ru(BPY)_3$) and an oxidizer (sodium persulphate) compound (Fig. 2(A) and (B)). Blue light (Wavelength = 452 nm) is illuminated on the pre-gel solution to excite $Ru(BPY)_3$ resulting in the formation of permanent dityrosine bonds (Fig. 2(C), (D), and (E)) through tautomerization of tyrosine residues on the surface of the folded BSA proteins. This chemical crosslinking continues until a system-spanning percolated network is formed with a measured storage modulus on the order of kPa. A previous study investigated the

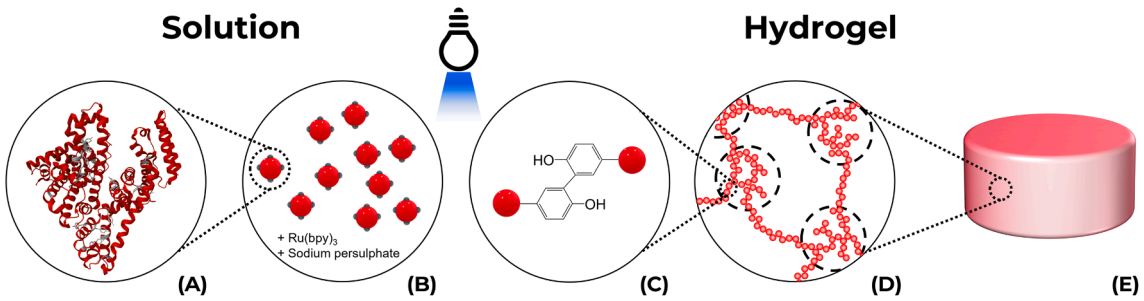

Fig. 2. Schematic showing folded protein hydrogels from nano to macro scales. (**A**) The crystal structure of BSA protein (PDB Code: 3 V03) depicted with tyrosine residues (crosslinking sites) highlighted in grey. (**B**) Globular BSA proteins resuspended in solution (plus the crosslinking reagents) (**C**) will become covalently bound to make a hydrogel initiated by 452 nm blue light. (**D** and **E**). (For interpretation of the references to colour in this figure legend, the reader is referred to the web version of this article.)

secondary structure of BSA proteins in photochemically crosslinked BSA hydrogels with circular dichroism using short path cuvettes and found the majority of BSA proteins (around 90% for $\phi = 7.4\%$) remain folded in photochemically crosslinked BSA hydrogels [14]. Thus, we assume proteins similarly remain predominantly folded in this study.

3.2. Rheology reveals a two-regime scaling behaviour for folded protein hydrogels

In situ gelation, using a custom-built lamp on the rheometer provides a time sweep of protein network formation and relaxation [16]. An example time sweep of the storage modulus is shown in Fig. 3(A) for a BSA hydrogel at $\phi = 3.7\%$. After a period of one minute, the lamp is switched on and the pre-gel solution begins to form crosslinks and percolate, resulting in an increase in the shear modulus. After 5 min, the lamp is switched off and the network relaxes, observed as a decay in the shear modulus with time reaching a plateau storage modulus, denoted $G'(t = \infty)$. The gel formation and relaxation for different ϕ are shown in Fig. 3(B). This indicates a successful manipulation of hydrogel mechanics with $G'(t = \infty)$ ranging from 0.07 kPa to 3.3 kPa by varying ϕ from low to high concentrations (light to dark shading respectively in the figure). Moreover, two different trends can be observed in this figure. Starting from $\phi = 1.5\%$, a rapid growth in the plateau storage modulus occurs when the concentration is slightly increased, and this growth slows down (as will become clearer in Fig. 4 below) from $\phi = 3.0\%$ to the maximum concentration value *i.e.*, $\phi = 7.4\%$ showing a scaling behaviour between $G'(t = \infty)$ and ϕ.

Such behaviour was also observed in the storage modulus of BSA protein hydrogels as a function of frequency for different protein ϕ (Fig. 4(A)). Each sample displays a weak positive power law which is characteristic of gel-like behaviour; plus, the scaling-like behaviour is preserved across the measured frequency range signifying it is not a frequency-dependent feature of the gels.

The above mechanical scaling findings are summarized in a double logarithmic plot of plateau storage modulus against ϕ (Fig. 4(B)). Initially, with increasing ϕ, significantly stronger gels are observed in the power law dependency (Eq. (1)) with the exponent $\mu_1 = 5.08 \pm 0.73$. At $\phi = 3.0\%$ and above, the mechanical enhancement becomes more gradual with a slope of the line in a log–log plot of $\mu_2 = 1.02 \pm 0.09$. Such two regime dependency of $G'(t = \infty)$ to ϕ is reminiscent of the flocculated theory described by Shih *et al.* [43] which will be discussed in detail later in this article.

Furthermore, to understand the viscoelastic behaviour of folded BSA hydrogels, the loss factor (tan (δ)) of these hydrogels is shown against ϕ in Supplementary Fig. 6. In this figure, tan (δ) progressively decreases as a result of increasing the concentration of BSA. Such behaviour implies that hydrogels with higher ϕ dissipate the energy less. This behaviour might be expected as the amount of solid particles (mainly BSA protein as the building block) is higher in more concentrated hydrogels thereby enhancing the elastic contribution to the gels viscoelastic behaviour.

3.3. Mesoscale structure of folded protein hydrogels using small angle neutron scattering

SANS is a powerful method to study the structure of protein hydrogels and gain mesoscale structural information [56,66,67]. The

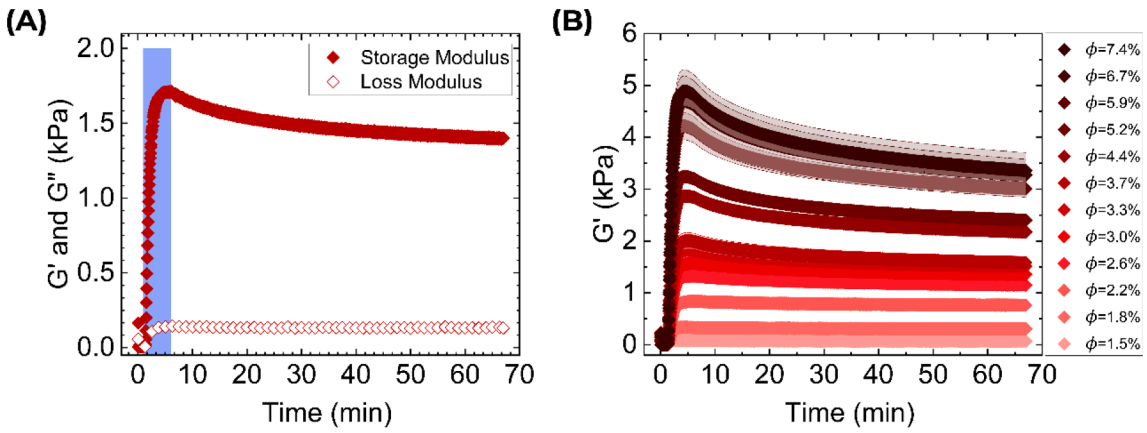

Fig. 3. Time sweep rheology of folded protein hydrogels in a concentration dependent study. (**A**) An example of the shear rheology of gel at $\phi = 3.7\%$, frequency = 1 Hz, and 0.5% shear rate showing G' and G'' as a function of time. After one minute, the in-situ lamp is switched on causing a significant enhancement in shear response of the gel. This rapid formation is followed by a slow relaxation until the system approaches a plateau storage modulus. The blue rectangular region shows the time range when the lamp was on. (**B**) The time dependency of BSA hydrogels is displayed for all the tested ϕ in this study from lowest ϕ shown (light shading) to dark shading for higher ϕ. (For interpretation of the references to colour in this figure legend, the reader is referred to the web version of this article.)

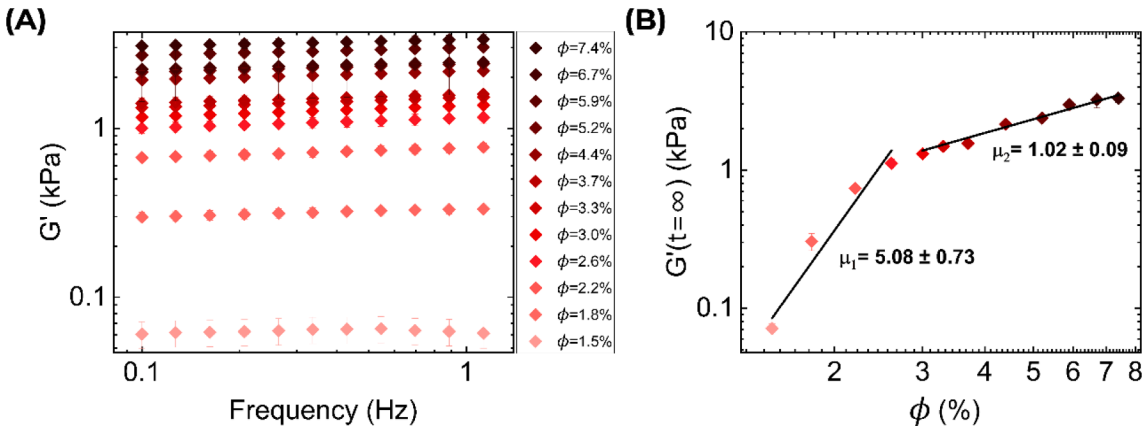

Fig. 4. Mechanical scaling of folded BSA gels. (A) The frequency dependence of each ϕ for folded BSA hydrogel shows a weak power law which implies a gel-like rheological response. Importantly, the same trend of growth of G' can be seen as Fig. 3(B) consistent for the whole range of frequencies. (B) Scaling of $G'(t=\infty)$ as a function of ϕ resembles two power laws with exponents $\mu_1 = 5.08 \pm 0.73$ and $\mu_2 = 1.02 \pm 0.09$.

scattering data for BSA hydrogels of varying ϕ are shown in Fig. 5(A) and (B). For the maximum BSA concentration ($\phi = 7.4\%$), the scattering curve shows a plateau region at low q (also known as Guinier region, ~0.002 to 0.008 $Å^{-1}$) followed by a power law reduction in the mid q region (~0.008 to 0.100 $Å^{-1}$) until the curve flattens again at high q (~0.100 to 0.5 $Å^{-1}$). As the concentration of BSA in the gel decreases, the curves' shape changes where the low q flat region shifts to lower q-values until it is completely outside of the q-range of the instrument (meaning we are unable to capture the Guinier region as the curves no longer show a plateau region at low q) and its intensity increases. Such

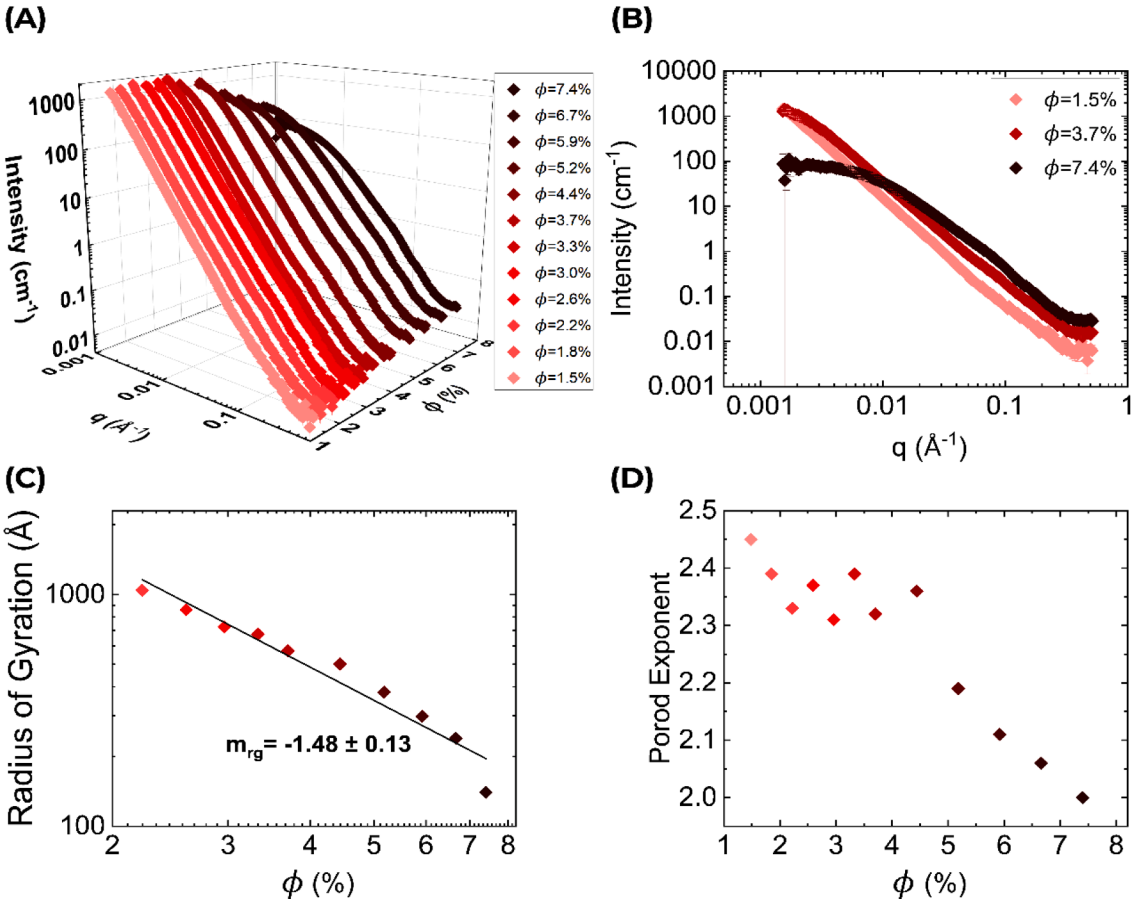

Fig. 5. SANS data obtained for different BSA ϕ and model-independent analysis. (**A**) A 3D graph showing the SANS curves for different volume fractions of BSA protein from $\phi = 1.5\%$ to 7.4%. (**B**) Scattering intensity versus q for three chosen volume fractions ($\phi = 1.5\%$, 3.7%, and 7.4%) to highlight the differences between structures. (**C**) Plot of radius of gyration,R_g, extracted from SANS curves (subfigure (A)) as a function of ϕ resembles a power law decay with slope of $m_{rg} = -1.48 \pm 0.13$ (the data points of $\phi = 1.5\%$ and 1.8% are omitted as the plateau region is too narrow to reliably fit). (**D**) Porod exponent shown as a function of ϕ. A stable fluctuation of Porod exponent is visible around ~ 2.4 and from $\phi = 5.2\%$ is shown to decrease reaching a value of 2.0. Note that error bars are smaller than the symbols in (**C**) and (**D**).

observation shows that the size of the largest mass assemblies inside the mesoscale network is increasing as the BSA ϕ is reduced. In addition, lowering ϕ results in a gradual increase in the slope of the mid q region which ceases around $\phi = 4.4\%$.

To understand the observed differences in network structure by varying ϕ, we perform Guinier-Porod fits to the SANS data to extract the radius of gyration (R_g) of the largest scattering objects (in this case, assemblies of proteins not the individual proteins) and the Porod exponent in the low and mid q regions, respectively. Fig. 5(C) shows R_g as a function of the building block concentration following a power law decay. Such continual reduction of the largest assemblies in the hydrogel network demonstrates these objects continue to decrease in size with increasing ϕ, a characteristic scaling behaviour anticipated by the blob and floc models which will be discussed later.

Further, the evolution of the Porod exponent with ϕ (Fig. 5(D)) gives information on how the geometry of the largest structure in the network changes with building block concentration. At lower ϕ, the exponent fluctuates around a constant value, then undergoes a continuous decay for $\phi \geq 5.2\%$. Porod exponents between 1 and 3 can be interpreted as a measure of the level of space-filling (which can be thought of as structure compactness), with larger values being indicative of greater space-filling (*e.g.*, a densely packed polymer has a Porod exponent of 3, while an extended Gaussian chain has a Porod exponent of 1.67). In folded protein hydrogels, this exponent is indicative of the complexity of the largest assemblies in the gel, related to D. Here, the value of Porod exponent from $\phi = 1.5\%$ to 4.4% is $\sim$ 2.4 which suggests the largest scattering objects share the same complexity of filling the space, while gels with higher volume fraction ($5.2\% \leq \phi \leq 7.4\%$) form less ramified assemblies. Thus, these results demonstrate that, at higher concentrations, folded protein hydrogels form smaller and less dense structures. In addition, the scattering curve of a BSA solution at $\phi = 2.2\%$ (30 mg/ml BSA solution) is provided in Supplementary Fig. 4. Performing a Guinier Porod fitting on this curve yields a R_g of 26.01 ± 0.06 Å in agreement with previous studies [68] which reported $R_g = 29 + 1$ Å at 4 mg/ml.

To further explore the details of the structure of folded protein hydrogels as a function of ϕ, we apply a previously presented [14,20,21] fractal structure factor model (**Materials and Methods**) which describes the protein network as fractal-like clusters of folded proteins linked together by an intercluster region. We extract the evolution of key structural parameters with increasing ϕ: the correlation length, ξ, which is related to the size of the clusters; the proportion of proteins in fractal-like clusters, P_c; and fractal dimension, D.

Fig. 6(A) shows a log–log graph of ξ versus ϕ. The maximum value of the correlation length is $\xi = 2266.30 \pm 373.02$ Å at $\phi = 2.2\%$ and decreases in a power law fashion to reach $\xi = 127.08 \pm 0.98$ Å at the highest BSA concentration $\phi = 7.4\%$. This inverse power law growth is consistent with Guinier analysis (Fig. 5(C)) and suggests that the cluster size inversely scales with the concentration of the building block. In addition, plotting P_c and D as a function of protein ϕ can reveal more about the network structure (Fig. 6(B)). To understand the behaviour of P_c better, it was fitted by a quadratic function. By doing so, the ϕ corresponding to the minimum value in P_c could be determined as $\phi_{critical} = 4.4\%$. For $\phi \leq \phi_{critical}$, the proportion of proteins occupying clusters decreases with ϕ, suggesting that increasing the concentration of BSA leads to a larger proportion of proteins in the intercluster region. However, this decay is reversed for gels with a protein concentration of $\phi > \phi_{critical}$ as they display an up-turn in P_c which suggests a change in the properties of the intercluster region. The fractal dimension from $\phi = 1.5\%$ to 4.4% fluctuates around a constant value ($D \sim 2.35$). Further increase of ϕ lead to a progressive reduction in the fractal dimension reaching $D = 2.06 \pm 0.01$. Indeed, a similar pattern for the Porod exponent was observed (Fig. 5(D)), which confirms the validity of D calculated using the fractal structure factor. It is interesting that the trend for both D and P_c alter at the same value of BSA ϕ.

By assuming a fractal structure factor model and extracting a number radial distribution function (**Materials and Methods**), we can extract more structural information about the protein network. The first parameter is defined as the number of proteins inside an average-sized cluster (N_{ave}) and is plotted in Fig. 7(A). N_{ave} displays a power law decay which is independent of P_c's sudden increase (Fig. 6(B)) and again follows a scaling behaviour. From this, the radius of an average cluster (r_c) is obtained and plotted in Supplementary Fig. 7. We observe that r_c follows a similar power law behaviour in agreement with R_g and ξ. Finally, the number density of average clusters (N_c) or simply the number of clusters in a unit volume was obtained and plotted in Fig. 7 (B). N_c displays a power law growth against BSA ϕ. It is apparent that, increasing BSA ϕ from 2.2% to 7.4% $\left(\frac{7.4\%}{2.2\%} = 3.63\right)$ can result in scaling of the population of clusters around 5000-fold more in a specific volume.

3.4. Scaling laws applied to folded protein hydrogels

Next, we consider the data in the context of scaling relationships based on the blob (polymers) and floc (colloids) models. Colloidal systems are formed by transient physical aggregation of globular particles while polymer systems which are composed of large and long building

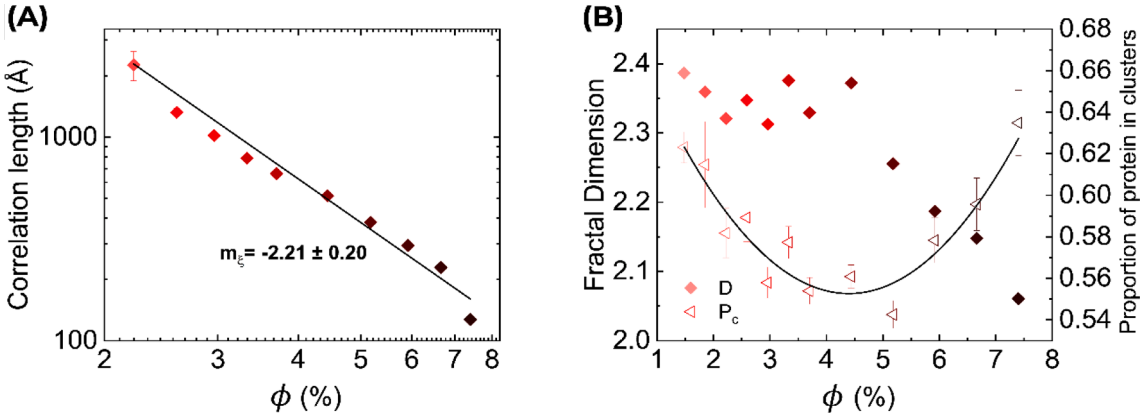

Fig. 6. Results from fitting SANS curves by a network of fractal clusters. (A) The power law decay of correlation length, ξ as a function of ϕ. Correlation length ξ is a characteristic length to determine the upper limit above which the fractality starts to drop and is closely related to the size of clusters. The trend of ξ closely follows R_g (Fig. 5(C)) with a power law exponent of $m_\xi = -2.21 \pm 0.20$. (B) The evolution of D and P_c with ϕ shows D is fluctuating around a constant value for $\phi \leq 4.4\%$ and declines for more concentrated gels. P_c is fitted by a quadratic function and the concentration increase leads to a reduction in its value until $\phi = \phi_{critical} = 4.4\%$, after this, the pattern alters, and the clusters begin to get more proteins in them as ϕ gets closer to its maximum value. $\phi = 1.5\%$ and 1.8% are not included in ξ correlation length fittings due to lack of data in the Guinier region.

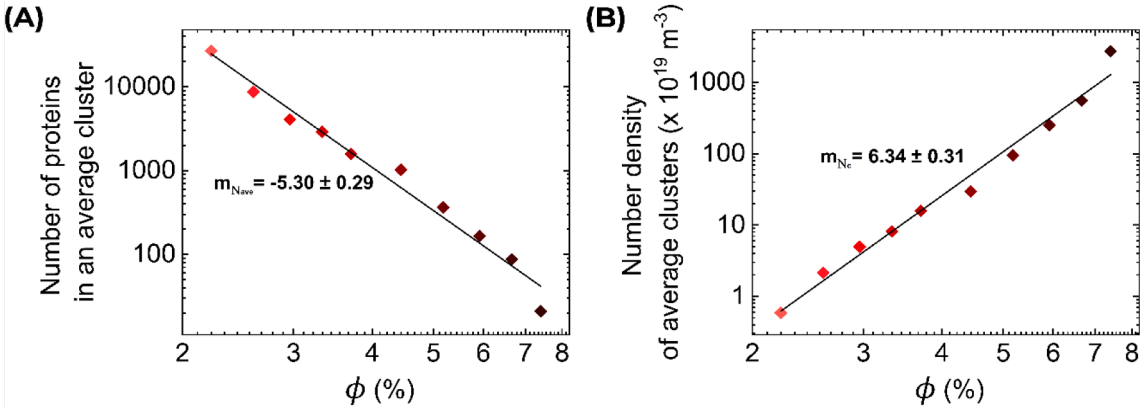

Fig. 7. Calculations of the fractal-like cluster network model assuming a radial distribution function. (**A**) The number of proteins in an average-sized cluster (N_{ave}) decreases in a power law fashion against ϕ (**B**) The number density of average-sized clusters (N_c) versus ϕ shows an increase in the number of clusters in a specific volume of space.

block chains with less convoluted structures are often made by chemical crosslinking. Since folded BSA hydrogels are composed of globular proteins (the geometry of the building block is similar to colloids), and they are made by permanent chemical crosslinking; they may be considered as an intermediate class of material which shares features of both polymer and colloidal gels and as a result, both polymer and colloidal scaling laws may be applicable.

As shown in Fig. 4(B), the scaling of the $G'(t=\infty)$ of folded protein hydrogels with ϕ exhibited two power laws. A two-power law dependency has previously been suggested for flocculated colloidal gel theory where at low ϕ, flocs are large and are more liable to bend thus defining- or dominating- the shear response while interflocs are harder to bend. A regime of strong interflocs is called the strong link and a higher value of μ (Eq. (3)) is expected. As the particle ϕ is increased, the flocs grow smaller and the interfloc links can bend more easily compared to the flocs. Thus, the interconnecting links are weaker in this regime called the weak link, with lower μ (Eq. (5)). To determine such regimes, one can take advantage of the difference between the sign of γ_0 in Eqs. (4) and (6). Inspired by this, we have extracted γ_0 and shown it in a double-logarithmic plot in Supplementary Fig. 8. Ideally, if the two regimes are present, first, a power law reduction for λ would occur (Eq. (4)) representative of the strong link followed by a discontinuity in the trend that is an increase in γ_0 representative of the weak link (Eq. (6)). However, despite seeing two power laws for the storage modulus (Fig. 4 (B)), no meaningful trend is observed for γ_0. The γ_0 is the shear rate above which the crosslinks break. Originally this was defined by Shih *et al.* as the point where in a rheology shear strain sweep test, a 5% deviation from the linear regime occurs. However, with BSA as the building block, the nonlinear regime may be the result of protein unfolding rather than the breakage of the bonds between the protein particles. Indeed, this may explain why such hydrogels show a shear-stiffening behaviour in a shear amplitude sweep study (Supplementary Fig. 9**)** and γ_0 does not follow the expected power law trends. Similar challenges associated with γ_0 can be found in the literature for denatured BSA protein hydrogels where only the increase (or the decrease) in γ_0's trend is considered to define the regime. In addition, when Wu and Morbidelli were attempting to test their modified scaling model (including a transition regime) [56] using Hagiwara *et al.*'s data [34], a data point was omitted in order to obtain a realistic value for γ_0. Here due to the complication with γ_0, possibly due to having folded proteins building up the gel, we cannot distinguish the regimes with certainty. Nonetheless, the existence of two distinct power laws with expected exponent values, in addition to the similarity between the structural models, can be regarded as having both regimes in the rather wide range of concentrations used in this paper. Hence, we chose $1.5\% \leq \phi \leq 2.6\%$ as the strong link regime and $\phi \geq 3.0\%$ as the weak link regime as they yield power laws with expected exponents.

Having defined the two concentration regimes, it is possible to extract D by fitting the scaling expressions in Eqs. (3) and (5) to the low and high concentration data, respectively. For the strong link regime, and given λ could not be reliably estimated, it is necessary to estimate the fractal dimension of the load-bearing backbone of the clusters, x. In general, x can vary, reaching a value close to D, yet, in the literature a narrow range of x $(1 < x < 1.3)$ has been used [56] and we have adopted the same approach. Choosing both limits of this range for $\mu_1 = 5.08 \pm 0.73$ yields a fractal dimension of $2.15 \pm 0.11 < D < 2.21 \pm 0.12$. For the weak link regime, Eq. (5) is enough to extract D, thus $\mu_2 = 1.02 \pm 0.09$ gives $D = 2.02 \pm 0.09$ which is surprisingly lower than the strong link regime. Rather unusually, these values are lower compared to the D obtained from the SANS data (~2.35, in the range where D is stable) (Fig. 6(B)). This suggests that there is some mechanism which supresses the system's mechanical growth with BSA concentration (causing a smaller power law exponent) resulting in a smaller fractality compared to scattering.

Eqs. (3), (4), (5), and (6) share the fundamental assumption that all gels have the same fractality, D. While previous studies have explored the different regimes, little is known about considering an upper limit for the weak link's regime. Perhaps, the general expectation is once the fractality drops, signatures would be visible in the mechanical measurements. This appears not to be the case for folded protein hydrogels. In fact, SANS has shown that D for $\phi > 4.4\%$ continuously decreases. This, however, does not disrupt the presence of a shallow power law as a sign of the weak link regime (Fig. 4(B)). If we choose $\phi = 4.4\%$ as an upper limit for the weak link *i.e.*, choosing the volume fraction range in which the fractal dimension from SANS fluctuates around a constant value, $(3.0\% \leq \phi \leq 4.4\%)$, a slightly steeper scaling exponent is obtained which is $\mu_3 = 1.30 \pm 0.08$ (Supplementary Fig. 10). Re-calculating the weak link's D leads to a value of $D = 2.23 \pm 0.21$. This is rather significantly bigger than D of the weak link with the wider ϕ range and very close to the higher end of the strong link regimes' D. Thus, care must be taken particularly in the weak link regime as the upper limit is difficult to ascertain for folded protein hydrogels without SANS knowledge.

Additionally, plotting the ratio of correlation length to the radius of protein ($r_0 \sim 3.5\ nm$) in Supplementary Fig. 11 reveals that at $\phi = 7.4\%$ the distance where a cluster possesses the same fractality decreases to only roughly four times the protein's radius. This may explain why D cannot be preserved for high BSA ϕ as clusters are not capable of producing the same convoluted assembly. The effect of this on rheological measurements, as explained above, was a weaker power law for the weak link regime.

Fig. 5(C) and 6(A) show that R_g and ξ both exhibit similar scaling

with ϕ. Such scaling decay is expected for the blob [32] and floc models [69] where

$$\xi_b \sim \phi^{\frac{\nu}{1-3\nu}} \tag{12}$$

$$\xi_f \sim \phi^{\frac{1}{D-3}} \tag{13}$$

where the subscripts b and f denote the blob and floc model, respectively. The number of monomeric units inside a blob is related to ν which is equal to $\frac{1}{D}$ [26,70,71], by applying this to Eq. (12), both above equations become the same.

The same approach could be taken for the number of proteins inside an average cluster. The blob model predicts the number of monomers in a blob (g_N) to decrease in a scaling power law as [32]:

$$g_N \sim \phi^{\frac{-1}{3\nu-1}} \tag{14}$$

In Eq. (14), g_N stands for the number of monomers making up a blob. Replacing ν as $\frac{1}{D}$ and g_N by N_{ave}:

$$N_{ave} \sim \phi^{\frac{D}{D-3}} \tag{15}$$

One can equate these exponents to the slope of ξ and N_{ave} to calculate D. This approach assumes that D remains constant, which is not observed in the SANS data (Fig. 6(B)). Nevertheless, despite the differences between the proposed model for protein hydrogels (simple chains in the intercluster region) with the blob model and the change of D beyond $\phi = 4.4\%$, power law scaling behaviours remain valid over the total range of ϕ.

While Eqs. (12), (13), and (15) show fractality-dependent relationships in a concentration study, scaling behaviours seen in the mesoscale structure of the system persist irrespective of the change in D. It might be expected that mechanical measurements are more affected by the change in D. Therefore, we can conclude the structural scaling relationships follow the same trend although the protein network space is confined, and the fractal-like clusters are unable to grow within the confined space to form the same fractality. On the other hand, the slope of the weak link (Fig. 4(B)) is affected by the drop in D, resulting in a smaller value of D in the region ($3.0\% \leq \phi \leq 7.4\%$).

4. Conclusion

We have presented a volume fraction, ϕ, dependent study of the mechanics and mesoscale structure of photochemically crosslinked folded BSA hydrogels reavealing scaling relationships in the measured range of ϕ. Rheological measurements confirm the existence of a two-regime power law scaling behaviour between shear storage modulus and ϕ. Using a fractal-like connected cluster model, we obtain information about the system's mesoscale network structure as a function of ϕ. Based on the trends of D and P_c, the ϕ dependence could be divided into two ranges. From $\phi = 1.5\%$ to 4.4% (Fig. 8 (A)–(C)), higher numbers of clusters (Fig. 8(1)) are formed with similar fractality (Fig. 8 (2)) which become continuously smaller as ϕ increases (Fig. 8(3)); consequently, the number of proteins inside a cluster decreases (Fig. 7 (A)). The proteins which are not in the clusters may result in longer chains of monomers in the intercluster region (Fig. 8(4)). Secondly, in gels with ϕ higher than 4.4% (Fig. 8 (C)–(D)), the number of proteins inside an average cluster decreases (Fig. 7(A)), more clusters are formed in a unit of volume (Fig. 8(1)), and clusters continue to reduce in size (Fig. 8(3)), as was seen for $1.5\% \leq \phi \leq 4.4\%$. However, the reduced number of particles per cluster limits the scope for branching in the protein network, leading to a reduction in D (Fig. 8(2)). In addition, P_c increases (Fig. 8(4)).

Such observations can be interpreted as in the range of $\phi > 4.4\%$ the system is highly concentrated meaning the clusters −which tend to grow in number with ϕ- fill up the space logarithmically (Fig. 8(1)) and their size decreases following a power law decay (Fig. 8(3)). The confinement of space prevents the formation of mature clusters with the same fractality (Fig. 8(2)), and proteins populate the clusters (Fig. 8(4)). In other

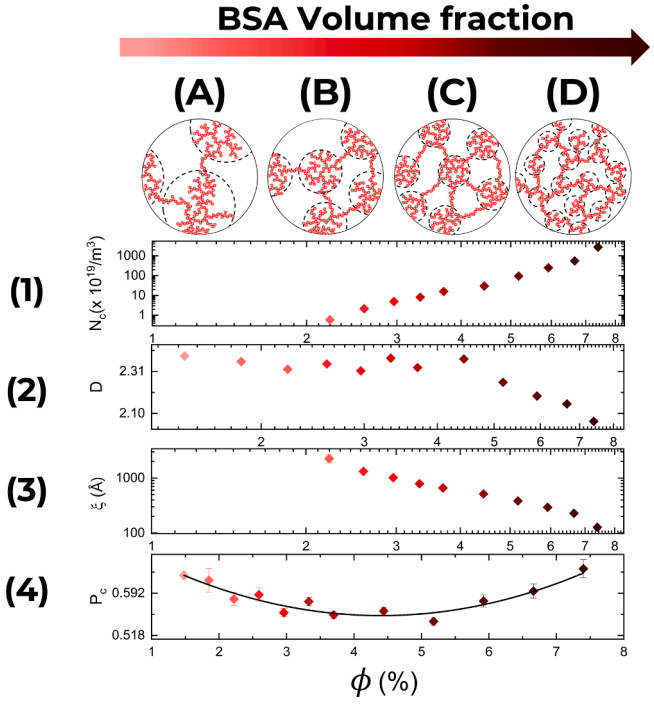

Fig. 8. A full understanding of the key parameters to depict the behaviour of protein hydrogels by varying the concentration of the building block. Parts (1)-(4) display N_c, D, ξ, and P_c as a function of ϕ, respectively. (A)–(D) shows the suggested schematic mesoscale representation of folded BSA hydrogels as ϕ increases. In the range of $1.5\% \leq \phi \leq 4.4\%$ ((A)–(C)), N_c increases in a power law fashion (1), D shows approximately a stable value (2), ξ decays logarithmically (3), and P_c reduces (4) all as a function of increasing ϕ. However, for $\phi > 4.4\%$ ((D)), D begins to decrease (2) P_c grows (4), with bigger population of clusters (1) which are sparser and smaller (3). This shows that further increase in the ϕ leads to a population of small clusters which do not share the same D and the intercluster proteins decrease.

words, at high ϕ, there is a finite amount of building block materials for clusters to absorb, grow, and mature. This is supported by Supplementary Fig. 11 where it is demonstrated that protein hydrogels with $\phi > 4.4\%$ have $\frac{\xi}{r_0} \leq 10$ meaning that the correlation length is on the order of the radius of the proteins. Such observation provides more evidence that at higher ϕ there is less space for proteins to assemble into more complex clusters and consequently, they will lose their ability to form the same fractality as lower ϕ. Such interpretation of the system's behaviour implies that the heterogeneity of the gels is decreasing towards $\phi = 7.4\%$.

Encouraged by the analogies between the mesoscale structure of folded protein networks and the blob and floc models, we determined scaling laws. For the mechanics of the BSA gels [43] a strong link regime ($1.5\% \leq \phi \leq 3.0\%$) was identified with a protein network ($\mu_1 = 5.08 \pm 0.73$) composed of large clusters with a fractal dimension range of $2.15 \pm 0.11 < D < 2.21 \pm 0.12$, which are interconnected by strong links. In $3.0\% \leq \phi \leq 7.4\%$, a weak link regime was observed with a power law of $\mu_2 = 1.02 \pm 0.09$ yielding $D = 2.02 \pm 0.09$. Nevertheless, SANS data indicates D is constant only in the range of $1.5\% \leq \phi \leq 4.4\%$. If this is considered, *i.e.* assuming an upper limit for the weak link's regime that is $3.0\% \leq \phi \leq 4.4\%$, the slope of the weak link increases to $\mu_3 = 1.30 \pm 0.08$ yielding $D = 2.23 \pm 0.21$. Such value is close to the upper end value estimated from the strong link *i.e.*, 2.21 ± 0.12. So, it appears that the fall in D does not disrupt the existence of a power law in the weak link regime, but it will decrease the slope value. Therefore, one should be cautious of using scaling relationships solely based on rheology. Another observation is that Shih's model provides D lower than what we determine from SANS ($D \sim 2.35$).

The power law behaviours extracted from the SANS data yield structural parameters such as ξ (Fig. 6(A)), N_{ave}, N_c (Fig. 7), and r_c (Supplementary Fig. 7). The blob and floc models predict such scaling relationships in Eqs. (12), (13), and (15). It is worth noting that the scaling models assume that the flocs/blobs are connected directly to each other (no inter floc/blob region is explicitly defined in these models), unlike the structural model of the protein network which points to the importance of an intercluster region between the fractal-like clusters. The structural model provided in this paper assumes some of the proteins reside outside of the fractal-like clusters defined as intercluster proteins. This may be the reason the floc model, which divides the mechanical behaviour into two regimes, is a better choice to model the mechanical response of the system. Whereas, the blob model predicts one power law for the mechanics of the system. The intercluster region therefore appears to be decisive for the mechanics of the folded protein hydrogels for higher ϕ. In addition, it is challenging to picture polymeric chains forming a convoluted pattern with $D \geq 2$. However, the scaling relationships (floc model for the mechanics and blob model for the structure) seem to be valid despite these differences, meaning the same predictions could be made for folded protein hydrogels cluster-related parameters to scale with ϕ. Another point to consider while using these models for folded protein hydrogels is that D will change at $\phi > 4.4\%$ while both models assume a constant value for D. So, one should be cautious of this drop in D while using them. This interesting observation might mean that the assembly of the clusters inside the network for $\phi > 4.4\%$ follows the same pattern as the more dilute hydrogels, however, the confinement of the space does not allow them to reach the same level of fractality. Modelling that explicitly represents the intercluster regions, while allowing mass transfer from clusters to intercluster regions and *vice versa*, may be necessary to establish scaling laws for folded protein hydrogel networks.

Lastly, we have shown that the structural data is well described by the blob model, while the rheological measurements follow the floc model. Such distinction between the structure and mechanics of the system can be related to previous work which has attempted to rationalize the origin of the mechanics of colloidal systems based on the microscopic and mesoscopic network heterogeneity [72–75]. For example, Zaccone *et al.*, showed intercluster contributions are critical to define the shear response of a structurally heterogenous system which is different to a homogenous glass system by orders of magnitude [73]. Here, we have highlighted this difference by demonstrating a cross-length scale behaviour of folded protein hydrogels in which clusters dominate the structure of the network while the intercluster region —in the weak link regime— plays a role in the mechanics. Further, the presence of repeating mesoscopic units in the heterogeneous structure of the system namely clusters enables the possibility of finding scaling relationships [72]. Such scaling relationships are invaluable for the development of applied biomaterials as the predictability of the mechanical and structural properties enables the development of tailored hydrogels with specific desired properties for drug delivery and other specialised biomedical applications.

CRediT authorship contribution statement

Ahmad Boroumand: Writing – review & editing, Writing – original draft, Methodology, Investigation, Formal analysis, Data curation, Conceptualization. **Matt D.G. Hughes:** Writing – review & editing, Methodology, Investigation, Formal analysis, Data curation. **Sophie Cussons:** Writing – review & editing, Methodology, Investigation, Data curation. **Najet Mahmoudi:** Writing – review & editing, Methodology, Investigation, Formal analysis, Data curation. **David A. Head:** Writing – review & editing, Supervision, Methodology, Investigation, Conceptualization. **Sally Peyman:** Writing – review & editing, Supervision, Methodology, Investigation. **Arwen I.I. Tyler:** Writing – review & editing, Supervision, Methodology, Investigation, Conceptualization. **Lorna Dougan:** Writing – review & editing, Validation, Supervision, Resources, Methodology, Investigation, Funding acquisition, Conceptualization.

Data availability

The data can be found at https://doi.org/10.5518/1638.

Declaration of competing interest

The authors declare that they have no known competing financial interests or personal relationships that could have appeared to influence the work reported in this paper.

Acknowledgements

The project was supported by a grant from the European Research Council (ERC) (UKRI EP/X023524/1) and the Engineering Physical Sciences Resaerch Council (EPSRC) (EP/ P02288X/1) to L. Dougan. We acknowledge ISIS Neutron and Muon Source for access to the Sans2d beamline (experiment number RB 2410269). This work benefitted from SasView software, originally developed by the DANSE project under NSF award DMR-0520547. Many thanks to all members of the Dougan group for helpful discussion and feedback.

Appendix A. Supplementary data

Supplementary data to this article can be found online at https://doi.org/10.1016/j.jcis.2025.138149.

Data availability

Data will be made available on request.

References

[1] J. Wu, et al., *Rationally designed synthetic protein hydrogels with predictable mechanical properties*, Nat. Commun. 9 (1) (2018) 620.

[2] H. Laurent, D.J. Brockwell, L. Dougan, *Nanomachine Networks: Functional All-Enzyme Hydrogels from Photochemical Cross-linking of Glucose Oxidase*, Biomacromolecules (2025).
[3] M.D. Hughes, et al., *Competition between cross-linking and force-induced local conformational changes determines the structure and mechanics of labile protein networks*, J. Colloid Interface Sci. 678 (2025) 1259–1269.
[4] D. Katrantzi, et al., Unveiling the structure of protein-based hydrogels by overcoming cryo-SEM sample preparation challenges, Faraday Discuss. (2025).
[5] L. Fu, et al., *Cartilage-like protein hydrogels engineered via entanglement*, Nature 618 (7966) (2023) 740–747.
[6] S. Lv, et al., *Designed biomaterials to mimic the mechanical properties of muscles*, Nature 465 (7294) (2010) 69–73.
[7] L. Fu, et al., *Dynamic protein hydrogels with reversibly tunable stiffness regulate human lung fibroblast spreading reversibly*, Chem. Commun. 55 (36) (2019) 5235–5238.
[8] L.R. Khoury, I. Popa, *Chemical unfolding of protein domains induces shape change in programmed protein hydrogels*, Nat. Commun. 10 (1) (2019) 5439.
[9] P. Ball, *The shape of things*, Nat. Mater. 23 (5) (2024) 578.
[10] M.D. Hughes, et al., *Building block aspect ratio controls assembly, architecture, and mechanics of synthetic and natural protein networks*, Nat. Commun. 14 (1) (2023) 5593.
[11] P. Fratzl, R. Weinkamer, *Nature's hierarchical materials*, Prog. Mater Sci. 52 (8) (2007) 1263–1334.
[12] F.M. Gartner, E. Frey, *Design principles for fast and efficient self-assembly processes*, Phys. Rev. X 14 (2) (2024) 021004.
[13] M.D. Hughes, et al., *Tuning protein hydrogel mechanics through modulation of nanoscale unfolding and entanglement in postgelation relaxation*, ACS Nano 16 (7) (2022) 10667–10678.
[14] M.D. Hughes, et al., *Control of nanoscale in situ protein unfolding defines network architecture and mechanics of protein hydrogels*, ACS Nano 15 (7) (2021) 11296–11308.
[15] M.D. Hughes, et al., *Single molecule protein stabilisation translates to macromolecular mechanics of a protein network*, Soft Matter 16 (27) (2020) 6389–6399.
[16] A. Aufderhorst-Roberts, et al., *Reaction rate governs the viscoelasticity and nanostructure of folded protein hydrogels*, Biomacromolecules 21 (10) (2020) 4253–4260.
[17] B.S. Hanson, L. Dougan, *Network growth and structural characteristics of globular protein hydrogels*, Macromolecules 53 (17) (2020) 7335–7345.
[18] B.S. Hanson, L. Dougan, *Intermediate structural hierarchy in biological networks modulates the fractal dimension and force distribution of percolating clusters*, Biomacromolecules 22 (10) (2021) 4191–4198.
[19] C. Huerta-López, et al., *Cell response to extracellular matrix viscous energy dissipation outweighs high-rigidity sensing*, Sci. Adv. 10 (46) (2024) eadf9758.
[20] M.D. Hughes, et al., *Capturing dynamic assembly of nanoscale proteins during network formation*, Small (2024) 2407090.
[21] C.P. Brown, et al., *Structural and mechanical properties of folded protein hydrogels with embedded microbubbles*, Biomater. Sci. 11 (8) (2023) 2726–2737.
[22] S.-H. Chen, J. Teixeira, *Structure and fractal dimension of protein-detergent complexes*, Phys. Rev. Lett. 57 (20) (1986) 2583.
[23] R. Mout, et al., *De novo design of modular protein hydrogels with programmable intra- and extracellular viscoelasticity*, Proc. Natl. Acad. Sci. 121 (6) (2024) e2309457121.
[24] T.L. Rapp, C.A. DeForest, *Tricolor visible wavelength-selective photodegradable hydrogel biomaterials*, Nat. Commun. 14 (1) (2023) 5250.
[25] J.A. Shadish, G.M. Benuska, C.A. DeForest, *Bioactive site-specifically modified proteins for 4D patterning of gel biomaterials*, Nat. Mater. 18 (9) (2019) 1005–1014.
[26] D. Johansen, J. Trewhella, D.P. Goldenberg, *Fractal dimension of an intrinsically disordered protein: Small-angle X-ray scattering and computational study of the bacteriophage λ N protein*, Protein Sci. 20 (12) (2011) 1955–1970.
[27] H. Hofmann, et al., *Polymer scaling laws of unfolded and intrinsically disordered proteins quantified with single-molecule spectroscopy*, Proc. Natl. Acad. Sci. 109 (40) (2012) 16155–16160.
[28] A. Milchev, *Single-polymer dynamics under constraints: scaling theory and computer experiment*, J. Phys. Condens. Matter 23 (10) (2011) 103101.
[29] D. Fritz, et al., *Multiscale modeling of soft matter: scaling of dynamics*, PCCP 13 (22) (2011) 10412–10420.
[30] S.R. Lustig, N.A. Peppas, *Solute diffusion in swollen membranes. IX. Scaling laws for solute diffusion in gels*, J. Appl. Polym. Sci. 36 (4) (1988) 735–747.
[31] P.-G. De Gennes, *Scaling concepts in polymer physics,* Cornell University Press, 1979.
[32] I. Teraoka, *Polymer solutions,* 2002.
[33] A. Stradner, P. Schurtenberger, *Potential and limits of a colloid approach to protein solutions*, Soft Matter 16 (2) (2020) 307–323.
[34] T. Hagiwara, H. Kumagai, T. Matsunaga, *Fractal analysis of the elasticity of BSA and β-lactoglobulin gels*, J. Agric. Food Chem. 45 (10) (1997) 3807–3812.
[35] T. Hagiwara, H. Kumagai, K. Nakamura, *Fractal analysis of aggregates in heat-induced BSA gels*, Food Hydrocoll. 12 (1) (1998) 29–36.
[36] R. Andoyo, et al., *Fractal dimension analysis of texture formation of whey protein-based foods*, Int. J. Food Sci. 2018 (1) (2018) 7673259.
[37] F. Bossler, et al., *Fractal approaches to characterize the structure of capillary suspensions using rheology and confocal microscopy*, J. Rheol. 62 (1) (2018) 183–196.
[38] Y. Isono, et al., *Viscoelastic properties of linear polymers with high molecular weights and sharp molecular weight distributions*, Macromolecules 11 (5) (1978) 888–893.
[39] K. Osaki, Y. Nishimura, M. Kurata, *Viscoelastic properties of semidilute polystyrene solutions*, Macromolecules 18 (6) (1985) 1153–1157.
[40] K. Osaki, et al., *The universality of viscoelastic properties of entangled polymeric systems*, Macromolecules 20 (3) (1987) 525–529.
[41] L. Bromberg, *Poly (ethylene oxide)-b-poly (propylene oxide)-b-poly (ethylene oxide)-g-poly (acrylic acid) copolymers as in situ gelling vehicle for nasal delivery*, in: *Modified-Release Drug Delivery Technology*, CRC Press, 2002, pp. 773–782.
[42] M.L. Oyen, *Mechanical characterisation of hydrogel materials*, Int. Mater. Rev. 59 (1) (2014) 44–59.
[43] W.-H. Shih, et al., *Scaling behavior of the elastic properties of colloidal gels*, Phys. Rev. A 42 (8) (1990) 4772.
[44] R. Buscall, et al., *Scaling behaviour of the rheology of aggregate networks formed from colloidal particles*, J. Chem. Soc., Faraday Trans. 1 84 (12) (1988) 4249–4260.
[45] S. Lazzari, et al., *Fractal-like structures in colloid science*, Adv. Colloid Interface Sci. 235 (2016) 1–13.
[46] T. Gisler, R.C. Ball, D.A. Weitz, *Strain hardening of fractal colloidal gels*, Phys. Rev. Lett. 82 (5) (1999) 1064.
[47] A. de Vries, et al., *Protein oleogels from heat-set whey protein aggregates*, J. Colloid Interface Sci. 486 (2017) 75–83.
[48] M.O. Eleya, S. Ko, S. Gunasekaran, *Scaling and fractal analysis of viscoelastic properties of heat-induced protein gels*, Food Hydrocoll. 18 (2) (2004) 315–323.
[49] S. Ikeda, E.A. Foegeding, T. Hagiwara, *Rheological study on the fractal nature of the protein gel structure*, Langmuir 15 (25) (1999) 8584–8589.
[50] L.G. Bremer, T. van Vliet, P. Walstra, *Theoretical and experimental study of the fractal nature of the structure of casein gels*, J. Chem. Soc., Faraday Trans. 1 85 (10) (1989) 3359–3372.
[51] L.G. Bremer, *Fractal aggregation in relation to formation and properties of particle gels,* Wageningen University and Research, 1992.
[52] P. Koshy, et al., *Unusual scaling in the rheology of branched wormlike micelles formed by cetyltrimethylammonium bromide and sodium oleate*, J. Phys. Chem. B 115 (37) (2011) 10817–10825.
[53] H. Fan, et al., *General rules for the scaling behavior of linear wormlike micelles formed in catanionic surfactant systems*, J. Colloid Interface Sci. 348 (2) (2010) 491–497.
[54] J. Jones, C. Marques, *Rigid polymer network models*, J. Phys. 51 (11) (1990) 1113–1127.
[55] F. MacKintosh, J. Käs, P. Janmey, *Elasticity of semiflexible biopolymer networks*, Phys. Rev. Lett. 75 (24) (1995) 4425.
[56] H. Wu, M. Morbidelli, *A model relating structure of colloidal gels to their elastic properties*, Langmuir 17 (4) (2001) 1030–1036.
[57] M. Verheul, et al., *Power law behavior of structural properties of protein gels*, Langmuir 14 (9) (1998) 2263–2268.
[58] A.C. Alting, et al., *Cold-set globular protein gels: Interactions, structure and rheology as a function of protein concentration*, J. Agric. Food Chem. 51 (10) (2003) 3150–3156.
[59] R. Wang, et al., *Decorating protein hydrogels reversibly enables dynamic presentation and release of functional protein ligands on protein hydrogels*, Chem. Commun. 55 (84) (2019) 12703–12706.
[60] Y. Song, et al., *Dual growth factor delivery using photo-cross-linkable gelatin hydrogels for effectively reinforced regeneration of the rotator cuff tendon*, ACS Appl. Bio Mater. 7 (2) (2024) 1146–1157.
[61] S. Haas, et al., *Changing mechanical properties of photopolymerized, dityrosine-crosslinked protein-based hydrogels*, Front. Bioeng. Biotechnol. 10 (2022) 1006438.
[62] D.T. Mildner, J. Carpenter, *Optimization of the experimental resolution for small-angle scattering*, J. Appl. Cryst. 17 (4) (1984) 249–256.
[63] O. Arnold, et al., *Mantid—Data analysis and visualization package for neutron scattering and μ SR experiments*, Nucl. Instrum. Methods Phys. Res., Sect. A 764 (2014) 156–166.
[64] A. Guinier, et al., *Small-angle Scattering of X-rays*, Wiley, New York, 1955.
[65] D.A. Fancy, T. Kodadek, *Chemistry for the analysis of protein–protein interactions: rapid and efficient cross-linking triggered by long wavelength light*, Proc. Natl. Acad. Sci. 96 (11) (1999) 6020–6024.
[66] R.B. Jadrich, D.J. Milliron, T.M. Truskett, *Colloidal gels*, J. Chem. Phys. 159 (9) (2023).
[67] S.F. Parker, P.J. Baker, R. McGreevy, *A vision for the future of neutron scattering and muon spectroscopy in the 2050s*, ACS Phys. Chem. Au (2024).
[68] J. Raw, et al., *Unveiling the three-step model for the interaction of imidazolium-based ionic liquids on albumin*, ACS Omega 8 (41) (2023) 38101–38110.
[69] G. Dietler, et al., *Gelation of colloidal silica*, Phys. Rev. Lett. 57 (24) (1986) 3117.
[70] S.M. Bhattacharjee, A. Giacometti, A. Maritan, *Flory theory for polymers*, J. Phys. Condens. Matter 25 (50) (2013) 503101.
[71] M. Rubinstein, R.H. Colby, *Polymer physics,* Oxford University Press, 2003.
[72] M. Bantawa, et al., *The hidden hierarchical nature of soft particulate gels*, Nat. Phys. 19 (8) (2023) 1178–1184.
[73] A. Zaccone, H. Wu, E. Del Gado, *Elasticity of arrested short-ranged attractive colloids: <? format?> homogeneous and heterogeneous glasses*, Phys. Rev. Lett. 103 (20) (2009) 208301.
[74] K.A. Whitaker, et al., *Colloidal gel elasticity arises from the packing of locally glassy clusters*, Nat. Commun. 10 (1) (2019) 2237.
[75] L. Di Michele, A. Zaccone, E. Eiser, *Analytical theory of polymer-network-mediated interaction between colloidal particles*, Proc. Natl. Acad. Sci. 109 (26) (2012) 10187–10192.